XN project: Brain CT Image Hemorrhage Segmentation

Wanning Zhou Lu Qian Yubing Gou
Department of Mathematics, Northeastern University

May 1, 2022

Abstract

Intracranial hemorrhage (ICH) is a life-threatening type of stroke, which requires fast and precise diagnosis. Nowadays, machine learning models are used widely in fastening and improving the decision-making process by taking input of computed tomography (CT) of the brain. These brain CT images come from patients who were diagnosed with single type of ICH, multiple types of ICH and without any sources of bleeding. After data cleaning, we ran three image classification models on 112,936 datasets. The data were split into training data, validation data and testing data with a splitting ratio of 80:10:10. The accuracies of these three models are below 30 percent. We then ran an image segmentation algorithm to predict the area of hemorrhage. The model accuracy reached 98.4 percent by applying U-net convolutional network architecture. This demonstrates the positive and efficient impact of machine learning techniques on medical image decision making.

1 Introduction

Intracranial hemorrhage (ICH), also known as cerebral bleed, is caused by bleeding within the brain tissue itself or between the brain tissue and skull. It is the second common cause of stroke, and it is a potential life-threatening medical emergency [1].

There are five different types of ICH based on the main areas where the bleeding occurs: either between the skull and brain tissue, or within the brain tissue. Three types of ICH can occur between the skull and brain tissue: Epidural hemorrhage, which happens between the skull bone and the dura mater; Subdural hemorrhage, which happens between the dura mater and the arachnoid membrane; Subarachnoid hemorrhage, which happens between the arachnoid membrane and the pia mater. Additionally, two types of ICH can occur inside the brain tissue: Intracerebral hemorrhage, which occurs anywhere inside the brain tissue itself; and Intraventricular hemorrhage, which occurs in the brain's ventricles [1]. Figure 1 is an example of brain CT scans of different types of ICH.

	Intraparenchymal	Intraventricular	Subarachnoid	Subdural	Epidural
Location	Inside of the brain	Inside of the ventricle	Between the arachnoid and the pia mater	Between the Dura and the arachnoid	Between the dura and the skull
Imaging	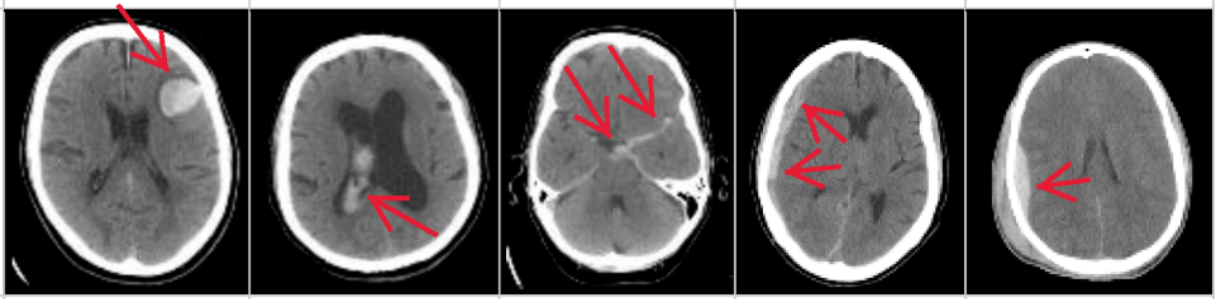				

Figure 1: *CT Scans of Different Types of ICH*

When a patient is brought to the emergency room with a suspected intracranial hemorrhage, Computed Tomography (CT) scan is typically used to help doctors detect the bleeding and make diagnosis for optimal treatments [2]. However, the diagnosis is complicated since it requires an accurate and immediate identification of the medical images in urgent situations.

In order to improve this process for effective treatment, we present three different machine learning models, including two convolutional neural network (CNN) models and one decision tree model to classify different types of ICH from brain CT scans. In addition, we also performed another CNN model for segmentation of the bleeding from the brain CT images.

2 Related work

In recent years, machine learning and deep learning approaches have been employed for a broad range of tasks in medical imaging, such as image classification and image segmentation.

Convolutional Neural Network (CNN) is one of the techniques which has been widely used for brain hemorrhage classification from CT scan images [3]. Some pretrained CNN models, such as AlexNet model [4] and ResNeXt-101 32×8 d model [5] were also applied for this task. In the base of CNN architecture, hybrid models such as AlexNet with support vector machine (AlexNet-SVM) [4], CNN with Long Short-Term Memory network (CNN + LSTM) [5][6], CNN with Gated Recurrent Unit (CNN + GRU) model [6] were performed as well. Besides the deep learning architectures, statistical machine learning classifier, such as Decision Tree, is another choice for detecting distinct types of hemorrhages efficiently [7]. Because of the variety of approaches, we decided to perform different models for the classification task.

Segmentation of medical images has been a challenging subject all the time. One important reason is that it demands a higher level of accuracy than what is desired in natural images [8]. The main idea of image segmentation is to group pixels in homogeneous regions and the usual approach to do this is by common features. In this case, the K-means clustering algorithm is widely used to segment the image [9]. At the same time, in the deep learning category, U-net architecture is one of the most used architectures for image segmentation. This method is widely used in different kinds of medical images. It also becomes a necessary step before medical diagnosis and treatment. For example, the authors use U-net to do the lung CT image segmentation to provide an accurate lung CT image analysis like lung cancer detection [10]. Also, there are still many classical segmentation architectures. FastFCN replaces dilated convolutions with the proposed JPU (Joint Pyramid Upsampling) module to reduce computation complexity [11]. Mask R-CNN is extended from Faster R-CNN by adding a branch for predicting segmentation masks on each Region of Interest (RoI). This approach efficiently detects objects in an image while simultaneously generating a high-quality segmentation mask for each instance [12]. We decided to use U-net architecture, as it is the most basic image segmentation model.

3 Classification

3.1 Data Introduction

3.1.1 Input Data

The dataset we used is provided by the Zeta Surgical company, which consists of various brain CT scan images. Each of the brain CT images contains a hemorrhage (bleeding) within it, which may contain only one type of hemorrhage, multiple types of hemorrhagesor normal brain CT scan without any hemorrhages. In this case, the hemorrhages are divided into 32 different types: intraparenchymal, intraventricular, subarachnoid, subdural, epidural, normal (six basic types) and all multiple combinations of different hemorrhages.

The CT scan images were provided from four different CT windows for each type of hemorrhages: brain bone window, brain window, max contrast window, and subdural window. However, only the CT images for brain window are used in this project for better results. An example of the brain CT image for brain window can be found below (Figure 2).

Figure 2: *Example of Brain CT Image from Brain window*

3.1.2 Target Values

The target values for the classification part are different types of hemorrhages, including single type of hemorrhages and all multiple combinations of hemorrhages. Table 1 is an example of the original file for the resulting types of hemorrhage, where "1" means that the image with given ID includes that particular type of hemorrhage, while "0" means it does not.

Image	any	epidural	intraparenchymal	intraventricular	subarachnoid	subdural
ID_00c33e2d9	1	1	1	0	0	0
ID_01fd04721	1	1	1	0	0	0
ID_020498ea7	1	1	1	0	0	0

Table 1: *Example of Original Results of Brain CT Images*

3.2 Data Preparation

3.2.1 Dataset Processing

After having a glance over the brain CT images, we found that some images were all black, which might affect the results. In this case, we manually removed the all-black CT images.

For the result file, we noticed that some data in the provided original file do not have corresponding brain CT images. We deleted this kind of data from the result file, so that each brain CT image matches with the corresponding type of hemorrhages. After cleaning the data, there are 112936 data left. Furthermore, we labelled the type names for each type of hemorrhages in the result file for convenience. For example, "epidural" represents the single epidural type of hemorrhage; "epi + subd" represents the combination of epidural and subdural types. Moreover, we assigned a unique number (from 0 to 31) to each type name for future work. Table 2 is an example of the final result file.

Image	any	epidural	intraparenchymal	intraventricular	subarachnoid	subdural	match	type	num_represent
ID_008da90f8	1	0	0	0	1	0	yes	subarachnoid	3
ID_18a19b529	1	0	1	0	1	0	yes	intrap + suba	11
ID_0e59726ca	1	0	0	1	1	0	yes	intrav + suba	13

Table 2: *Example of Final Results*

3.2.2 Data Selection

After the dataset processing step, we were able to see the distribution of the whole dataset. However, we can see from Figure 3 that the distribution of the whole dataset is imbalanced. After having a closer look at the data distribution (Table 3), we noticed that the number of patients experiencing from single type of hemorrhages (such as subdural, subarachnoid) are much higher than the number of patients suffering from multiple types of hemorrhages (such as epi + suba). For this reason, we decided to perform the hemorrhage classification in two different ways: one for classifying all types of hemorrhages (32 in total), and the other for classifying only single type of hemorrhages (6 in total).

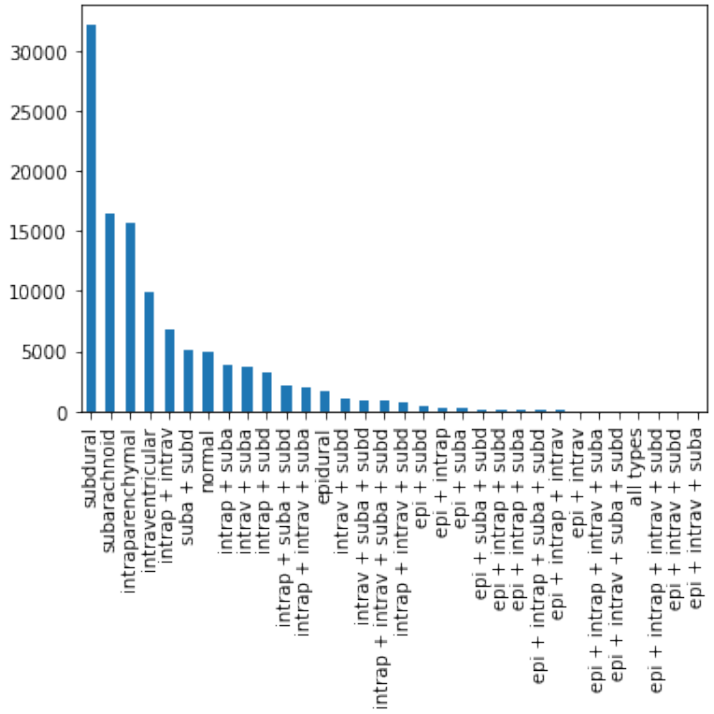

Figure 3: *Distribution of Whole Dataset*

subdural 32199	subarachnoid 16423	intraparenchymal 15661	intraventricular 9878	intrap + intrav 6817	suba + subd 5082
normal 5008	intrap + suba 3932	intrav + suba 3677	intrap + subd 3311	intrap + suba + subd 2198	intrap + intrav + suba 1955
epidural 1693	intrav + subd 1084	intrav + suba + subd 968	intrap + intrav + suba + subd 871	intrap + intrav + subd 728	epi + subd 382
epi + intrap 281	epi + suba 220	epi + suba + subd 108	epi + intrap + subd 93	epi + intrap + suba 88	epi + intrap + suba + subd 52
epi + intrap + intrav 50	epi + intrav 40	epi + intrap + intrav + suba 36	epi + intrav + suba + subd 30	all types 23	epi + intrap + intrav + subd 19
epi + intrav + subd 17	epi + intrav + suba 12				

Table 3: *Detailed Distribution of Whole Dataset*

In the case of classifying all the types of hemorrhages, we used 500 data for each type of hemorrhages based on the detailed distribution showed in Table 3. And in the case of classifying only single type of hemorrhages, we used 1600 data for each type based on the distribution shown in Table 4.

epidural	intraparenchymal	intraventricular	subarachnoid	subdural	normal
1693	15661	9878	16423	32199	5008

Table 4: *Distribution of Single Type of Hemorrhages*

3.2.3 Image Processing

After selecting the data we would use based on the distribution, we performed the image processing step before fitting different machine learning models. This step includes image cropping, image resizing, image augmentation and image normalization.

The original size of each CT image is (512, 512, 3). Since there are some black areas in each image which might affect the results, we decided to crop all images by only keeping the middle 350×350 to get rid of the black areas.

In addition, since we plan to fit some pretrained CNN architectures in the future, we resized the images from size (512, 512, 3) to size (224, 224, 3), which are suitable to be inputted into most pretrained architectures.

Data augmentation was also performed because the size of the dataset we would use is not big enough. It was performed randomly by the following transformations:

- Height shift with maximum 0.1 percent of the image
- Rotation with maximum 20 degrees
- Width shift with maximum 0.1 percent of the image
- Zoom with maximum of 0.2 percent of the image
- Randomly flip the image horizontally

Figure 4 shows an example of the original sample image and the one after cropping and resizing. The image pixels were then normalized to the range [0, 1] by dividing 255.

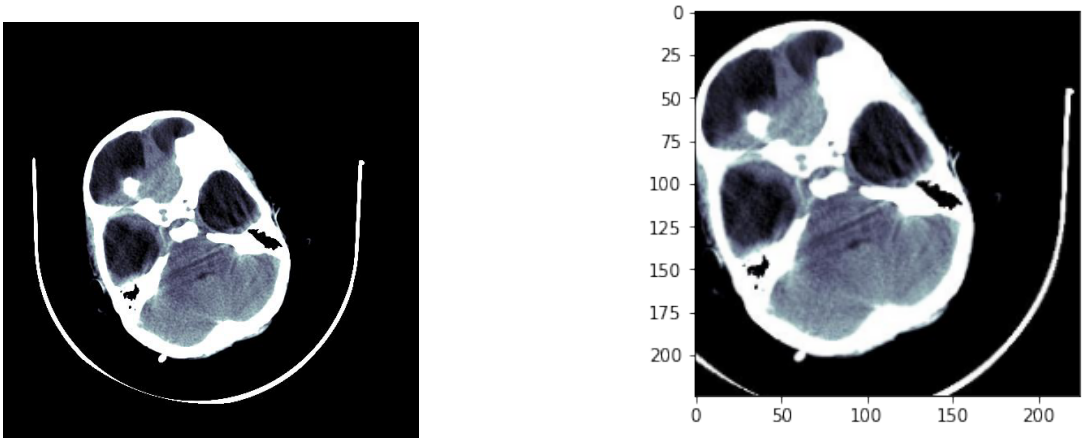

Figure 4: *Original Sample Image (Left) and the One After Cropping and Resizing (Right)*

3.2.4 Testing/Training Split

For both classifying all types of hemorrhages and classifying single type of hemorrhages, we used 80 percent of the dataset for training, 10 percent of the dataset for validating, and 10 percent of the dataset for testing.

3.3 Methodology

We applied three different machine learning models for classifying all types of hemorrhages and classifying only single type of hemorrhages respectively, which includes one simple Convolutional Neural Network (CNN) model, one pretrained CNN model – ResNet50, and one Decision Tree model.

3.3.1 Convolutional Neural Network (CNN) Model

The first model we used is a simple CNN model, and the input size is (224, 224, 3). The architecture for this model is as following:

1. Conv 2D: 32 filters, Kernel (7×7), 'ReLu', Padding 'valid'
2. Max Pooling 2D: Pooling size (2×2)
3. Conv 2D: 32 filters, Kernel (3×3), 'ReLu'
4. Max Pooling 2D: Pooling size (2×2)
5. Dropout: Dropout rate (0.25)
6. Flatten Layer
7. Dense Layer: 128 units, 'ReLu'
8. Dropout: Dropout rate (0.5)
9. Dense Layer: 32 units (number of total types), 'Softmax' (for all types)

   Or: 6 units (number of single types), 'Softmax' (for single types only)

This model was trained using RMSprop as optimizer, categorical cross entropy as loss. Class weight was also set to this model in case of the imbalanced data.

Figure 5 shows the accuracies and losses for classifying all types of hemorrhages after 20 epoches. The accuracy for testing data is about 0.0592, and the loss is about 3.4572.

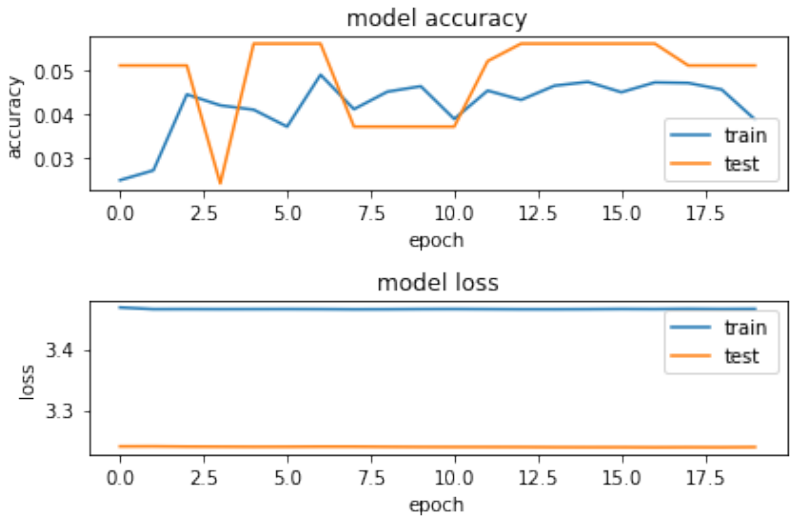

Figure 5: *Accuracies and Losses for Classifying All Types Using Simple CNN Model*

Figure 6 shows the accuracies and losses for classifying only single type of hemorrhages after 20 epoches. The accuracy for testing data is about 0.166, and the loss is about 1.792.

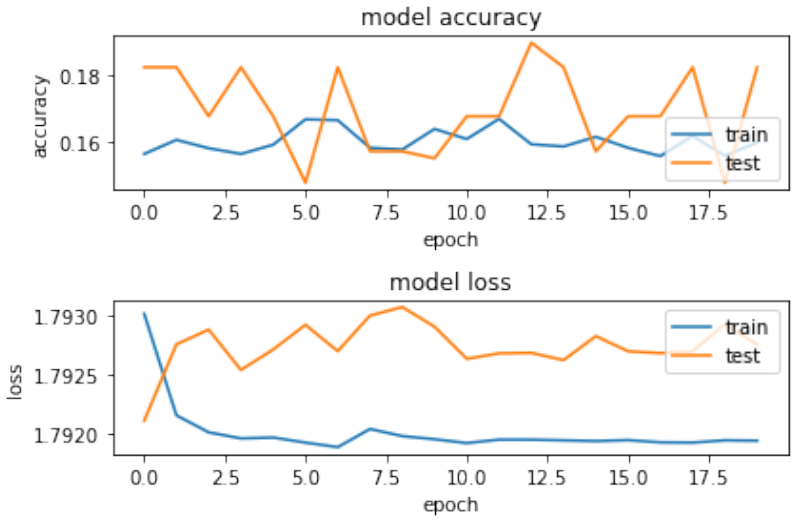

Figure 6: *Accuracies and Losses for Classifying Single Type Using Simple CNN Model*

The accuracies for both classifying all types of hemorrhages and only single type of hemorrhages are low. However, the one for only classifying single type is higher than the one for classifying all types by comparison.

3.3.2 ResNet-50 Model

The second model we used is the ResNet-50 model, which is a pretrained CNN model. Figure 7 shows the architecture of ResNet-50 model.

layer name	output size	18-layer	34-layer	50-layer	101-layer	152-layer
conv1	112×112	7×7, 64, stride 2				
conv2_x	56×56	3×3 max pool, stride 2				
		$\begin{bmatrix} 3\times3, 64 \\ 3\times3, 64 \end{bmatrix}\times2$	$\begin{bmatrix} 3\times3, 64 \\ 3\times3, 64 \end{bmatrix}\times3$	$\begin{bmatrix} 1\times1, 64 \\ 3\times3, 64 \\ 1\times1, 256 \end{bmatrix}\times3$	$\begin{bmatrix} 1\times1, 64 \\ 3\times3, 64 \\ 1\times1, 256 \end{bmatrix}\times3$	$\begin{bmatrix} 1\times1, 64 \\ 3\times3, 64 \\ 1\times1, 256 \end{bmatrix}\times3$
conv3_x	28×28	$\begin{bmatrix} 3\times3, 128 \\ 3\times3, 128 \end{bmatrix}\times2$	$\begin{bmatrix} 3\times3, 128 \\ 3\times3, 128 \end{bmatrix}\times4$	$\begin{bmatrix} 1\times1, 128 \\ 3\times3, 128 \\ 1\times1, 512 \end{bmatrix}\times4$	$\begin{bmatrix} 1\times1, 128 \\ 3\times3, 128 \\ 1\times1, 512 \end{bmatrix}\times4$	$\begin{bmatrix} 1\times1, 128 \\ 3\times3, 128 \\ 1\times1, 512 \end{bmatrix}\times8$
conv4_x	14×14	$\begin{bmatrix} 3\times3, 256 \\ 3\times3, 256 \end{bmatrix}\times2$	$\begin{bmatrix} 3\times3, 256 \\ 3\times3, 256 \end{bmatrix}\times6$	$\begin{bmatrix} 1\times1, 256 \\ 3\times3, 256 \\ 1\times1, 1024 \end{bmatrix}\times6$	$\begin{bmatrix} 1\times1, 256 \\ 3\times3, 256 \\ 1\times1, 1024 \end{bmatrix}\times23$	$\begin{bmatrix} 1\times1, 256 \\ 3\times3, 256 \\ 1\times1, 1024 \end{bmatrix}\times36$
conv5_x	7×7	$\begin{bmatrix} 3\times3, 512 \\ 3\times3, 512 \end{bmatrix}\times2$	$\begin{bmatrix} 3\times3, 512 \\ 3\times3, 512 \end{bmatrix}\times3$	$\begin{bmatrix} 1\times1, 512 \\ 3\times3, 512 \\ 1\times1, 2048 \end{bmatrix}\times3$	$\begin{bmatrix} 1\times1, 512 \\ 3\times3, 512 \\ 1\times1, 2048 \end{bmatrix}\times3$	$\begin{bmatrix} 1\times1, 512 \\ 3\times3, 512 \\ 1\times1, 2048 \end{bmatrix}\times3$
	1×1	average pool, 1000-d fc, softmax				
FLOPs		1.8×10^9	3.6×10^9	3.8×10^9	7.6×10^9	11.3×10^9

Figure 7: *ResNet-50 Architecture*

A Flatten Layer and a Dense Layer with the number of types of hemorrhages were added over the ResNet-50 model, so that the shapes of output can match with the corresponding number of types of hemorrhages. In addition, layers in ResNet-50 model were freezed, but only the last added fully connected layers were trained.

This model was trained using Adam as optimizer, and sparse categorical cross entropy as loss. Class weight was also set to this model in case of the imbalanced data.

Figure 8 shows the accuracies and losses for classifying all types of hemorrhages after 10 epoches. The accuracy for testing data is about 0.0522, and the loss is about 4.133.

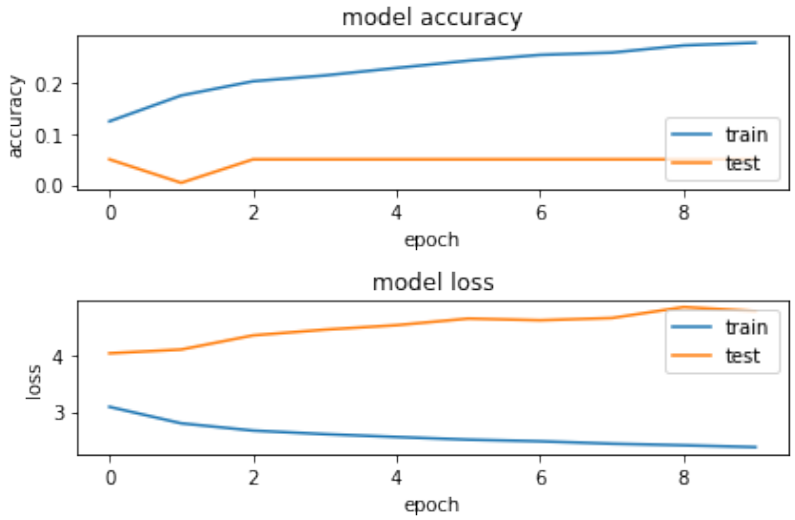

Figure 8: *Accuracies and Losses for Classifying All Types Using ResNet-50 Model*

Figure 9 shows the accuracies and losses for classifying only single type of hemorrhages after 10 epoches. The accuracy for testing data is about 0.142, and the loss is about 2.874.

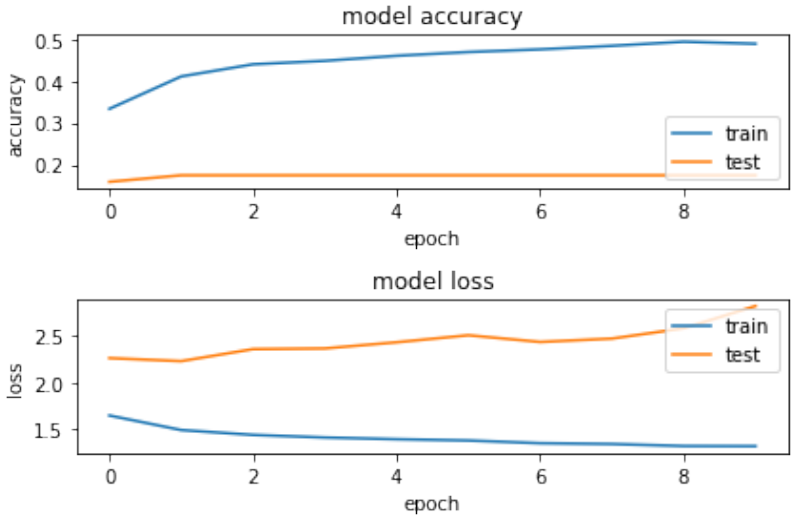

Figure 9: *Accuracies and Losses for Classifying Single Type Using ResNet-50 Model*

The accuracies for both classifying all types of hemorrhages and only single type of hemorrhages are a little bit lower than the ones using simple CNN model previously. However, the one for only classifying single type is higher than the one for classifying all types by contrast.

3.3.3 Decision Tree Model

Besides CNN models, we also tried the Decision Tree Model, which is another image classification technique. In the case of fitting the Decision Tree Model, we first need to convert our 4D array of dataset into a 2D array of dataset that the model expects.

For classifying all types of hemorrhages, the original shape of the input training data is (9951, 224, 224, 3) which is a 4D array. The first parameter represents the number of input data, and the second to the fourth parameters represent the shape of each image. The 2D array of dataset is achieved by reshaping the training data as (9951, $224 \times 224 \times 3$). And the resulting 2D array shape for training data is (9951, 150528). The same work was performed to the validation data and testing data. As a result, the validation dataset was converted from (995, 224, 224, 3) to (995, 150528), and the testing dataset was converted from (996, 224, 224, 3) to (996, 150528).

After this preprocessing step, we directly fit the dataset to the Decision Tree Classifier under sklearn library. As a result, the accuracy score for the validation data is about 0.1045, and the one for the testing data is about 0.08936.

For classifying only single type of hemorrhages, we followed the same process as for classifying all types of hemorrhages. The shape of input training data was reshaped from (7680, 224, 224, 3) to (7680, 150528), the shape of validation data was reshaped from (960, 224, 224, 3) to (960, 150528), and the shape of testing data was reshaped from (960, 224, 224, 3) to (960, 150528). After fitting the dataset to the model, the accuracy score for the validation data is about 0.265, and the one for testing data is 0.25.

Although the results are still poor, we can see that the accuracy for Decision Tree model is the highest among the three models we tried, and the ones for classifying only single type of hemorrhages are higher than the ones for classifying all types of hemorrhages.

4 Segmentation

According to the results we got by running image classification models, we found that the accuracy scores were all below 30 percent. Therefore, we determined to apply image segmentation model for predicting hemorrhage area.

4.1 Data Cleaning

The Zeta Surgical company provided 6 CSV files containing total of 5488 data in which the boundary coordinates of hemorrhages are labeled by the neurosurgeons.

According to the instructions, first, we deleted the data that "Correct Label" and "Majority Label" are both empty. Second, we chose "Correct Label" as the final label. If it does not exist, the "Majority Label" was applied instead. Third, the boundaries of hemorrhage area are labeled independently. If there are multiple hemorrhage areas in one CT scan image, they are labelled separately. To get the overall hemorrhage area for each patient, we integrated these different pieces together into a single image. As a result, 2788 images were ready to be segmented.

4.2 Image Segmentation

Same as image classification, we only used images from brain window directory to do the segmentation for the best results. We imported the data into Python and used Matplotlib library to visualize the outcomes. The first step we took was plotting the boundaries of hemorrhages using given labels. Then we highlighted the area with color. The second step was generating the mask area. In order to be fitted into the U-net architecture, we modified the pixels' values of the hemorrhage area to 1 (white), and other areas to 0 (black). Figure 10 is an example of the processed images. The leftmost image is the original image. The middle picture includes the hemorrhage area overlaid on the left one, where the green area represents the hemorrhage area. The rightmost image of Figure 10 shows the mask image. The final dataset consists of the original and mask image, which would all be inputted into U-net model.

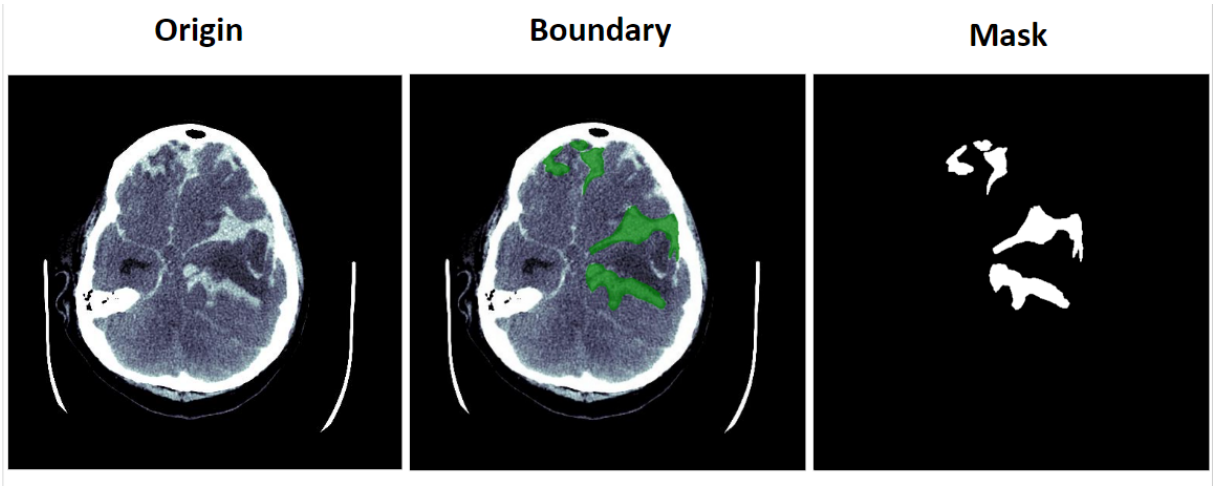

Figure 10: *Example of Image With Boundary and Mask*

To eliminate the influence of skull area to the model, we also removed the skull area during data preparation. Figure 11 is an example of the image after skull removal. We calculated the means and standard deviations of the original images. Then we used erosion and dilation function from Skicit-image package to remove the skull area. This also increased the image contrast, which makes the hemorrhage area more conspicuous. The images with skull removal would also be fitted into the U-net model for comparison.

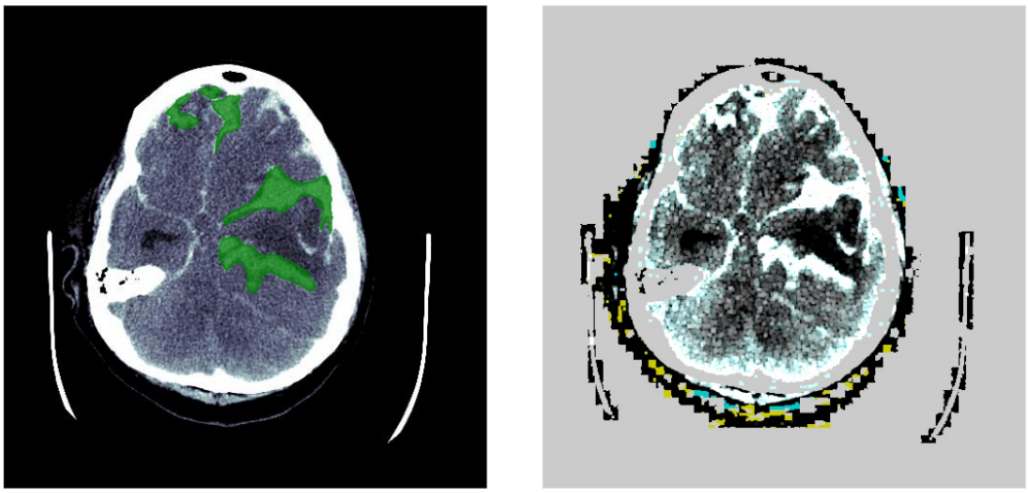

Figure 11: *Example After Removing Skull Area (Right)*

4.3 Methodology

We would use U-net convolutional neural network architecture for the image segmentation task. As we are trying to solve separating the area of hemorrhage and the background, it should be identified as semantic segmentation. Since the U-net architecture is designed for semantic segmentation, it is the most suitable model for us [13]. It learns segmentation in an end-to-end setting. The input data is the original CT scan image and the output is the mask of the image. Figure 12 shows an example of input and output images for U-net architecture:

Figure 12: *Input (Left) and Output (Right) Images for U-net Model*

4.4 U-net Architecture

The U-net model includes 2 paths, which are contraction path and expansion path. It includes convolution, max pooling and upsample operations. The brief structure of U-net architecture can be found in Figure 13.

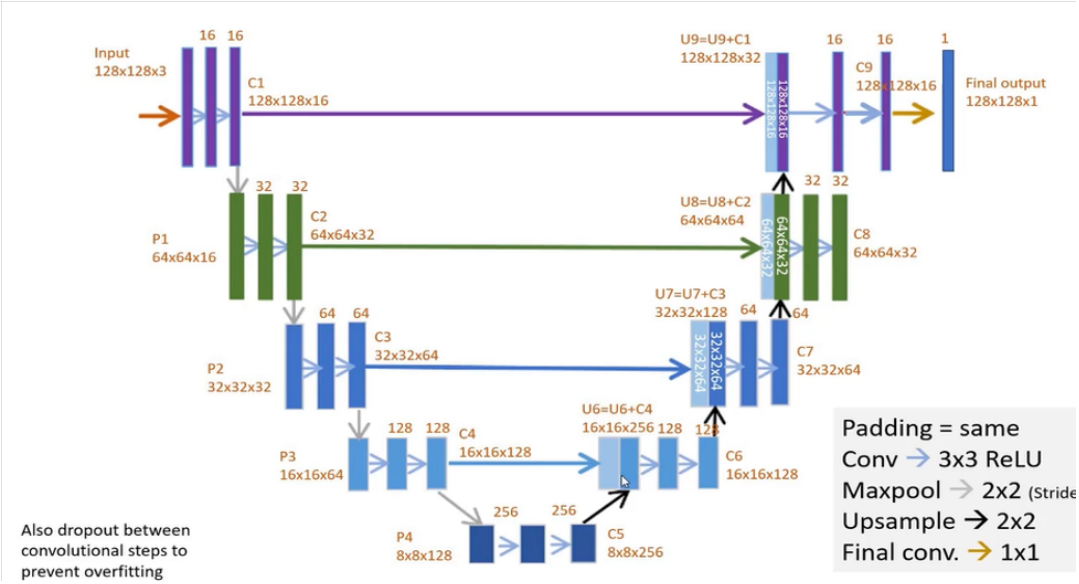

Figure 13: *U-net Architecture*

The architecture of the U-net model is set as following:
Contraction path:
1. Conv 2D: 16 filters, Kernel (3×3), 'ReLu', Padding 'same'
2.Dropout: Dropout rate (0.1)
3.Conv 2D: 16 filters, Kernel (3×3), 'ReLu', Padding 'same'
4.Max Pooling 2D: Pooling size (2×2)
5.Repeat

6.Conv 2D: 256 filters, Kernel (3 × 3), 'ReLu', Padding 'same'
7.Dropout: Dropout rate (0.3)
8.Conv 2D: 256 filters, Kernel (3 × 3), 'ReLu', Padding 'same'

Expansion path:
1.Upsample: 128 filters, Kernel (2 × 2), 'ReLu', Padding 'same'
2.Concatenate c4 and U6
3.Conv 2D: 128 filters, Kernel (3 × 3), 'ReLu', Padding 'same'
4.Dropout: Dropout rate (0.2)
5.Conv 2D: 128 filters, Kernel (3 × 3), 'ReLu', Padding 'same'
6.Repeat
7.Output layer: 16 filters, Kernel (3 × 3), 'ReLu', Padding 'same'

This model used Adam as optimizer, which involves a combination of 2 gradient descent methodologies, the momentum and root mean square propagation. The loss was calculated using binary cross entropy. The metrics we used to evaluate the model is 'accuracy'. After running 10 epochs with batch size as 32, the model reached 98.4 percent of accuracy with 90 percent training data and 10 percent testing data. The loss of the model is approximately 0.294. Figure 14 shows clearly about the accuracy and model loss for each epoch.

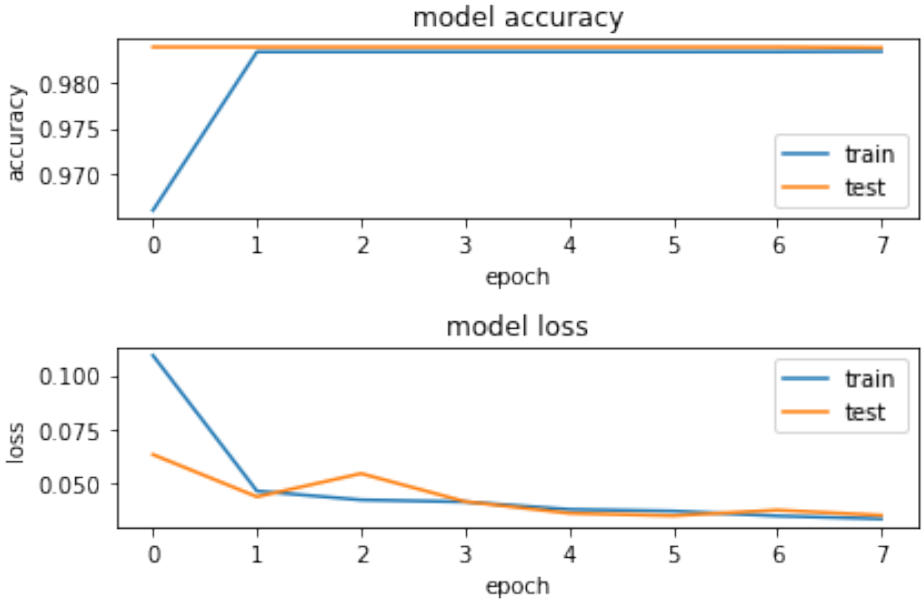

Figure 14: *Accuracies and Losses of U-net Model*

As a result, the accuracy of this model is high for image segmentation. An example of the predicted value is shown in Figure 15:

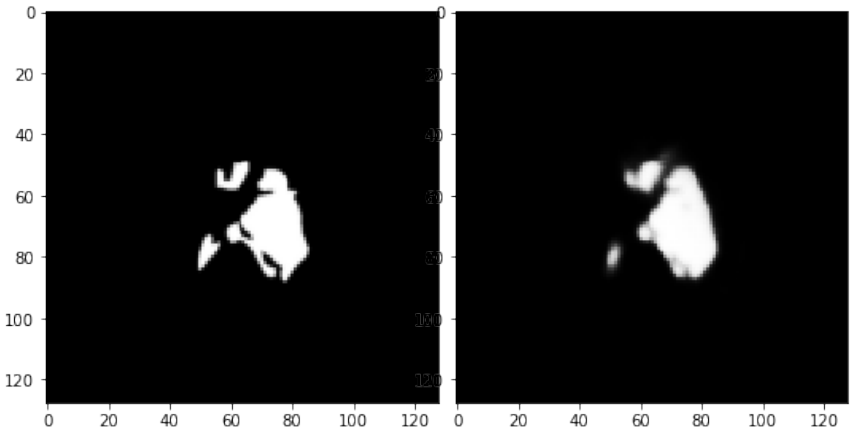

Figure 15: *Example 1 of Mask Area Plotted by Labels (Left) and Predicted Mask Area(Right)*

Figure 15 is a great example showing that we are able to predict the area of hemorrhages precisely. However, there are a few cases that the model gave a larger prediction area than the actual hemorrhage area. These cases would happen when there is no significant contrast between the hemorrhage area and the background. In this case, the model would predict the brain skull area as well. Figure 16 shows an example for this situation.

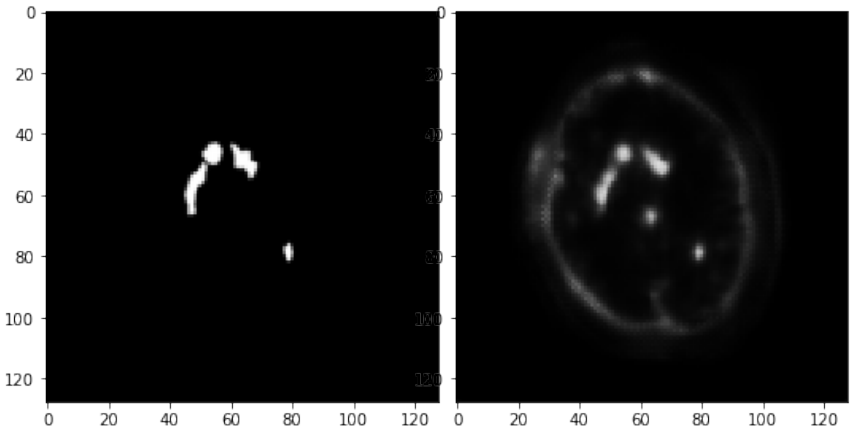

Figure 16: *Example 2 of Mask Area Plotted by Labels (Left) and Predicted Mask Area(Right)*

Because of these cases, we also tried reducing the impact of skull by removing the skull area and increasing the contrast (Figure 11). However, the result of the modified model has not improved as much as what we expected. Therefore, we kept using the original CT scan images as our input data.

Another metric that evaluates the image segmentation model is IoU (intersection over Union).

$$IoU = \frac{Intersection \cap Union}{Intersection \cup Union} \tag{1}$$

The IoU value for the first example (Figure 15) was high, but it was relatively very low for the second example (Figure 16) since the union area is much bigger. In other words, the IoU value for this model was greatly impacted by predictions like example 2 (Figure 16). For this reason, we did not use IoU as our evaluation metrics.

5 Results

5.1 Image Classification

The model accuracy and loss for each classification model are shown in Table 5.

Model	Accuracy (32 combinations)	Lost (32 combinations)	Accuracy (6 single types)	Lost (6 single types)
CNN	0.0592	3.4572	0.166	1.792
ResNet-50	0.0522	4.133	0.142	2.874
Decision Tree	0.08936		0.25	

Table 5: *Results for Classification Models*

It can be concluded that among these three models, the decision tree model is the most suitable classification model to predict hemorrhage type in our case. In addition, the accuracies of all three models are higher for classifying single type of hemorrhages than classifying all possible types.

5.2 Image Segmentation

The U-net model performed well in image segmentation task. It reached 98.4 percent of accuracy and the model loss is 0.284. In conclusion, U-net is a good tool to determine the hemorrhage area. Although the removal of skull area did not increase the model performance, there are a few steps we can try in the future for improvement.

5.3 Further improvement

First, the input data we used were only from the brain window directory. We can use images from the other three windows to test as we may miss some information by using images from single window. Secondly, there are a few other segmentation models we can try, such as FastFCN, Mask R-CNN and Gated-SCNN. Third, for the mask image, we only generated two layers, hemorrhage (white) and other area (black). We can segment the images into multiple layers, such as background, skull, hemorrhage and brain (four layers). Additionally, because of the limitations of our devices, the number of data we used was small, which might be the reason of poor results. By using better devices, we are able to train the models with more data which may lead to better results.

References

[1] "Brain bleed/hemorrhage (intracranial hemorrhage): Causes, symptoms, treatment," Cleveland Clinic. [Online]. Available: https://my.clevelandclinic.org/health/diseases/14480-brain-bleed-hemorrhage-intracranial hemorrhage. [Accessed: 30-Apr-2022].

[2] "Intracerebral hemorrhage (ICH), hemorrhagic stroke, stroke: Cincinnati, oh mayfield brain spine," , hemorrhagic stroke, stroke — Cincinnati, OH Mayfield Brain Spine. [Online]. Available: https://mayfieldclinic.com/pe-ich.htm. [Accessed: 30-Apr-2022].

[3] K.Jnawali, M.R.Arbabshirani, N.Rao, and A.A.P.M.D., "Deep 3D convolution neural network for CT Brain Hemorrhage Classification," SPIE Digital Library, 27-Feb-2018. [Online]. Available: https://www.spiedigitallibrary.org/conference-proceedings-of-spie/10575/105751C/Deep-3D-convolution-neural-network-for-CT-brain-hemorrhage-classification/10.1117/12.2293725.short?SSO=1. [Accessed: 30-Apr-2022].

[4] A. M. Dawud, K. Yurtkan, and H. Oztoprak, "Application of deep learning in neuroradiology: Brain Haemorrhage Classification Using Transfer Learning," Computational intelligence and neuroscience, 03-Jun-2019. [Online]. Available: https://www.ncbi.nlm.nih.gov/pmc/articles/PMC6589279/. [Accessed: 30-Apr-2022].

[5] M. Burduja, R. T. Ionescu, and N. Verga, "Accurate and efficient intracranial hemorrhage detection and subtype classification in 3D CT scans with convolutional and long short-term memory neural networks," Sensors (Basel, Switzerland), 01-Oct-2020. [Online]. Available: https://www.ncbi.nlm.nih.gov/pmc/articles/PMC7582288/. [Accessed: 30-Apr-2022].

[6] "BHCNet: Neural Network-based brain hemorrhage classification using head CT Scan," IEEE Xplore. [Online]. Available: https://ieeexplore.ieee.org/abstract/document/9507442. [Accessed: 30-Apr-2022].

[7] International Journal of Recent Technology and Engineering (IJRTE), 30-Apr-2022. [Online]. Available: https://www.ijrte.org/. [Accessed: 30-Apr-2022].

[8] Z. Zhou, M. M. R. Siddiquee, N. Tajbakhsh, and J. Liang, "UNet++: A nested U-Net Architecture for Medical Image segmentation," Deep Learning in Medical Image Analysis and Multimodal Learning for Clinical Decision Support : 4th International Workshop, DLMIA 2018, and 8th International Workshop, ML-CDS 2018, held in conjunction with MICCAI 2018, Granada, Spain, S..., Sep-2018. [Online]. Available: https://www.ncbi.nlm.nih.gov/pmc/articles/PMC7329239/R4. [Accessed: 30-Apr-2022].

[9] G. Sharmila and V. Valli Mayil, "Image Segmentation For CT Image With Artefac," ijser.org, Jul-2014. [Online]. Available: https://www.ijser.org/researchpaper/Image-Segmentation-For-CT-Image-With-Artefact.pdf. [Accessed: Apr-2022].

[10] B.A.Skourt, A.E.Hassani, and A.Majda,"Lung CT image segmentation using Deep Neural Networks," Procedia Computer Science, 12-Mar-2018. [Online]. Available: "https://www.sciencedirect.com/science/article/pii/S1877050918301157". [Accessed: 30-Apr-2022].

[11] H. Wu, J. Zhang, K. Huang, K. Liang, and Y. Yu, "FASTFCN: Rethinking dilated convolution in the backbone for semantic segmentation," arXiv.org, 28-Mar-2019. [Online]. Available: https://arxiv.org/abs/1903.11816. [Accessed: 30-Apr-2022].

[12] K. He, G. Gkioxari, P. Dollar, and R. Girshick, "Mask R-CNN," CVF Open Access, 01-Jan-1970. [Online]. Available: https://openaccess.thecvf.com/content-iccv-2017/html/He-Mask-R-CNN-ICCV-2017-paper.html. [Accessed: 30-Apr-2022].

[13] O. Ronneberger, P. Fischer, and T. Brox, "U-Net: Convolutional Networks for Biomedical Image Segmentation," SpringerLink, 01-Jan-1970. [Online]. Available: "https://link.springer.com/chapter/10.1007/978-3-319-24574-4-28." [Accessed: 27-Apr-2022].